symmetry

MDPI

Article

Covalently Bonded Fullerene Nano-Aggregates $(C_{60})_n$: Digitalizing Their Energy–Topology–Symmetry

Denis Sh. Sabirov [1,*], Ottorino Ori [2], Alina A. Tukhbatullina [1] and Igor S. Shepelevich [1,3]

[1] Laboratory of Mathematical Chemistry, Institute of Petrochemistry and Catalysis UFRC RAS, 450075 Ufa, Russia; kalieva.alina@rambler.ru (A.A.T.); shepelevichis@mail.ru (I.S.S.)
[2] Actinium Chemical Research Institute, 00182 Rome, Italy; ottorino.ori@gmail.com
[3] Bashkir State University, Bulletin of Bashkir University, 450076 Ufa, Russia
* Correspondence: diozno@mail.ru; Tel.: +7-347-284-27-50

Abstract: Fullerene dimers and oligomers are attractive molecular objects with an intermediate position between the molecules and nanostructures. Due to the size, computationally assessing their structures and molecular properties is challenging, as it currently requires high-cost quantum chemical techniques. In this work, we have jointly studied energies, topological (Wiener indices and roundness), and information theoretic (information entropy) descriptors, and have obtained regularities in triad 'energy–topology–symmetry'. We have found that the topological indices are convenient to indicating the most and least reactive atoms of the fullerene dimer structures, whereas information entropy is more suitable to evaluate odd–even effects on the symmetry of $(C_{60})_n$. Quantum chemically assessed stabilities of selected C_{120} structures, as well as linear and zigzag $(C_{60})_n$, are discussed.

Keywords: fullerene; fullerene dimers; fullerene oligomers; topological efficiency; Wiener index; information entropy; symmetry

Citation: Sabirov, D.S.; Ori, O.; Tukhbatullina, A.A.; Shepelevich, I.S. Covalently Bonded Fullerene Nano-Aggregates $(C_{60})_n$: Digitalizing Their Energy–Topology–Symmetry. *Symmetry* **2021**, *13*, 1899. https://doi.org/10.3390/sym13101899

Academic Editor: P. Ulrich Biedermann

Received: 4 August 2021
Accepted: 5 October 2021
Published: 9 October 2021

1. Introduction

Fullerene nanostructures constructed with two or more fullerene cages are promising all-carbon building blocks for nanoarchitectonics [1,2]. Dimers $(C_{60})_2$, regioisomeric $(C_{70})_2$, and cross-dimer C_{130} contain direct covalent bonding of the fullerene cages and are classic representatives of this type of exohedral fullerene derivatives [3]. Most studied experimentally, dimer $(C_{60})_2$ is formed by the solid-state mechanochemical [2+2]-cycloaddition reaction between the C_{60} cages [4,5]. This dimer has numerous structural isomers among the carbon framework nanostructures, such as the family of isomeric C_{120} fullerenes, the stability of which was theoretically explored [6–8], and peanut-shaped nanostructures with fused C_{60} cages [9]. The structures of [2+2]-$(C_{60})_2$ and C_{120} fullerenes contain pentagons and hexagons whereas the fusion of the cages in the peanut carbon nanostructures is due to the introduction of the heptagon–pentagon pairs.

More complex carbon nanostructures can be mechanochemically produced based on the abovementioned [2+2]-dimerization reaction [10]. These are, for example, regioisomeric C_{60} trimers [11], which were detected and then studied using direct visualization with scanning tunneling microscopy. Ohtsuki et al. have shown that the formation of the C_{60} and C_{70} tetramers were detected with the radiochromatographic technique [12]. The [2+2]-linked multicage fullerene compounds can be formed in the carbon nanotubes, which act as the nanoreactor providing pre-reaction self-assembly of the reactant and stabilizes the oligomerization/polymerization products [13–17]. Note that there are obstacles for the experimental studies of large fullerene oligomers associated with the low solubility.

There are many theoretical papers devoted to the structure–energy and structure–property relationships of the two- and multicage fullerene nanostructures [1,11,15–28]. In these works, mainly the quantum chemical techniques (e.g., density functional theory

methods, DFT) are applied to the fullerene dimer/oligomer nanostructures. However, a computational treatment of the fullerene multicage compounds with high-level methods is hard due to the large size of their molecules that makes the calculations time- and resource-cost.

The topological approach associated with the analysis of the molecular graphs and subsequent calculations of the topological descriptors has become an efficient method to study relative stability trends within the series of fullerene isomers (see [29] and references therein). Previous works exploited Wiener index and topological roundness parameters to study C_{60} [30], C_{28} [31], C_{66} [32], C_{76} [33], and C_{84} fullerene isomers [34,35], as well as nanocones [36]; and to monitor the Stone–Wales transformations of the giant C_{240} fullerene [37]. Thus, the approach works well in the case of diverse nanostructures containing 5-, 6-, 7-, and other cycles that make up their skeletons [30–37]. In the mentioned works, good correlations for fullerene structures were found between (a) the energy/molecular properties and topological roundness; and (b) sphericity and volume (geometry parameters) and topological roundness. It means that the topological approach could be used to pre-screen some structural, molecular, and physicochemical properties of the C_{60} oligomers without the necessity of heavy quantum chemical artillery, which may be further applied to refine the energy/molecular properties of a selected number of nanostructures. Meanwhile, the topological indices were not applied to the fullerene dimers and oligomers.

In the present work, we have combined quantum chemical and topological techniques to study the C_{60} dimers and oligomers and demonstrate the efficiency of the topological approach for scrutinizing their chemical structures.

2. Computational Details

All optimizations were performed by the density functional theory method PBE/3ζ implemented in the Priroda program [38]. The 3ζ basis set contains the orbital basis sets of contracted Gaussian-type functions (11s,6p,2d)/[6s,3p,2d], which are used in combination with the density-fitting basis sets of uncontracted Gaussian-type functions and (10s,3p,3d,1f) for carbon atoms. The hessians of the optimized structures contain no imaginary frequencies. The optimized geometries were used for the determination of their symmetry point groups in the ChemCraft program [39].

Note that C_{60} and its derivatives remains a challenge for computational studies due to the strong static correlation [40] and specific DFT-based methods are developed to take into account this feature [41–43]. The obstacles for correct description of the electron system of C_{60} assumedly relate the nonplanar displacement of sp^2-hybridized carbon atoms and symmetry effects [44]. This feature becomes less pronounced for C_{60} derivatives with reduced π-electron systems, so that 'classic' DFT methods may provide reliable results. The abovementioned method PBE/3ζ reproduces structures and physicochemical parameters of fullerene derivatives with high accuracy, including dimer and oligomers [21–23,45–50].

The essence of the topological approach is based on describing a carbon molecule on a simple graph $G(N,B)$, in which N vertices and B edges correspond to N carbon atoms and B chemical bonds, respectively. The vertices of $G(N,B)$ are labeled as V_i (i = 1, 2, . . . , N–1, N). The graphs present several invariants reflecting their topological structure. In particular, molecular descriptors deduced from the chemical distances d_{ij} between all couples of vertices V_i and V_j of $G(N,B)$ extract the information stored in the molecular topology. Chemical distance d_{ij} represents the length of the shortest path between vertices V_i and V_j by walking on molecular graph bonds, taking $d_{ii} = 0$. Then, transmission w_i on the node i is defined as (it assumes integer positive values):

$$w_i = \sum_j d_{ij}, \text{ with } j = 1, \ldots, N \quad (1)$$

The Wiener index $W(N)$ is the integer defined as the semi-sum of the chemical distances:

$$W(N) = \frac{1}{2}\sum_i w_i, \text{ with } i = 1, \ldots, N \quad (2)$$

and essentially provides a measure of the molecular compactness [51].

Graph invariants w_i give the contributions to $W(N)$ coming from nodes V_i. By indicating the eccentricities of the nodes as M_i and numbers of m-neighbors of V_i as b_{im}, we can rewrite the transmission in a more convenient form:

$$w_i = \sum_m m b_{im}, \text{ with } m = 1, \ldots, M_i \quad (3)$$

Integer values b_{im} are also called the Wiener weights of vertex V_i. Algorithmically, the upper limit M_i in the sum over m of Equation (3) may be changed into the graph diameter $M = max\{M_i\}$ for every node i with an appropriate usage of null Wiener weights, i.e., $b_{im} = 0,\ M_i < m \leq M$. The maximum distance present in graph diameter $G(N,B)$ is $M = max\{d_{ij}\}$. The extremal values of invariants w_i:

$$\underline{w} = min\{w_i\}, \text{ with } i = 1, \ldots, N \quad (4)$$

$$\overline{w} = max\{w_i\} \text{ with } i = 1, \ldots, N \quad (5)$$

characterize the most (less) embedded nodes of with the minimal $\underline{w}$ and maximal $\overline{w}$ transmission, respectively. This allows defining topological efficiency index ρ of the graph that measures the average gap among transmission of the vertices and the minimal vertex contribution $\underline{w}$ to $W(N)$:

$$\rho = \frac{2W(N)}{N\underline{w}} \text{ with } \rho \geq 1 \quad (6)$$

The extreme topological efficiency (or extreme topological roundness) ρ^E is simply defined as

$$\rho^E = \frac{max\{w_i\}}{min\{w_i\}} = \frac{\overline{w}}{\underline{w}} \text{ with } \rho^E \geq 1 \quad (7)$$

Invariants ρ and ρ^E are rooted into the topological symmetry of the nanostructure $G(N,B)$. In a set of similar graphs, they privilege systems with a high symmetry, i.e., with a value equal (or close) to 1.

3. Results and Discussion

3.1. The C_{120} Isomers: A Fullerene and Two Dimers

We have considered three isomeric all-carbon molecules to scrutinize the relations between the topology and other molecular properties. These are fullerene C_{120} (D_5) and two dimers, i.e., [2+2]-dimer $(C_{60})_2$ (C_{2h}) and fused dimer C_{120} (C_i), which have a peanut shape (hereinafter, the symmetry point groups of the molecules are shown in parentheses) (Figure 1). Note that the structures were theoretically studied (see, e.g., [6,9,20]) and their parameters found in the present work are in agreement with the previous works. In this work, we compare the thermodynamic favorability of the three isomers based on the quantum chemical total energies found:

$$\Delta E = E^{tot}_{C_{120}} - 2E^{tot}_{C_{60}}, \quad (8)$$

where $E^{tot}_{C_{60}}$ is the total energy of buckminsterfullerene C_{60} (I_h) (all E values include zero-point vibration energies). The estimates of Equation (8) are the energy effects of the formation reactions of the C_{120} isomers from C_{60} (I_h), the most abundant fullerene structure [52]. According to energy calculations (Table 1), the thermodynamic stability of the structures decreases in the series: C_{120} (D_5)–C_{120} (C_i)–$(C_{60})_2$ (C_{2h}), i.e., the fullerene molecule and the [2+2]-dimer are the most and the least favorable compounds of the series.

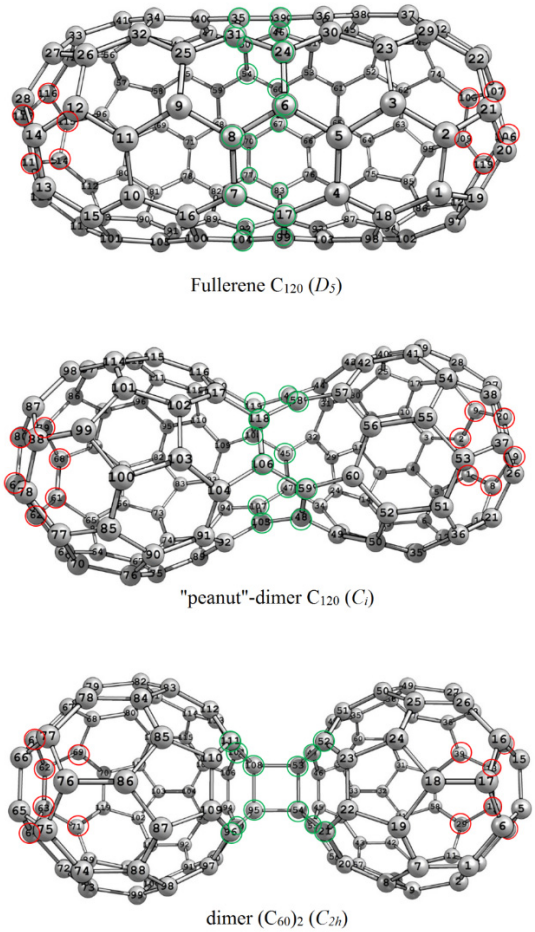

Figure 1. The C_{120} isomers with highlighted most and less topo-reactive atoms (read and green, respectively).

Table 1. Topology and energy parameters of the C_{120} isomers.

Isomer	ΔE (kJ/mol)	W	M	$\underline{w}$	$\overline{w}$	ρ	ρ^E
C_{120} (D_5)	−1170.1	48,820	15	366	460	1.1116	1.2568
C_{120} (C_i)	−149.2	49,362	16	333	497	1.2353	1.4925
$(C_{60})_2$ (C_{2h})	+11.4	51,912	18	308	548	1.4045	1.7793

All topological indices indicate that fullerene C_{120} is topologically favored among the nanostructures under study. Indeed, its molecule is the most compact (lowest W and graph diameter M) and the most round from the topological point of view (lowest ρ and ρ^E values) (Table 1).

As follows from the topological calculations, the three structures have the stable central belts, i.e., the atoms that should be less reactive due to their topological embedding. They are shown in green circles in Figure 1. The corresponding nodes are characterized with minimal transmission values $\underline{w}$ (Equation (3)). In contrast, maximal values ($\overline{w}$) indicate highly reactive atoms (in topological sense or 'topo-reactive'), which are highlighted with red circles in Figure 1. The $\underline{w}$ values show that the dimers have very stable nodes, e.g., four sp^3-hybridized carbon atoms of the cyclobutane ring bridging the fullerene cores in dimer $(C_{60})_2$ (C_{2h}). Dimer C_{120} (C_i) is characterized the higher $\overline{w}$ values that is interpreted as the corresponding nodes are 'topo-reactive' working against the global molecular stability. Note that we consider topological interactions that occur at any distance in the graph, i.e., every node interacts with all the other 119 nodes.

Thus, for the three C_{120} nanostructures, low topo-reactive atoms are located in the middle, forming a stability belt. As for experimental fullerene chemistry, this is consistent with the reactivity of fullerenes in the addition reactions, e.g., the addition of dipole molecules or radicals (in a less degree). For example, the reactivity of the atoms and 6.6-bonds of the C_{70} fullerene molecule decreases from poles to equator of the cage. Moreover, equatorial 6.6-bonds (traditionally designated as *ee*) do not even react with ozone, diazomethane, carbenes, peroxyl radicals etc. [53]. Obviously, this is due to the shift of the π-electron density, which is crucial for reactivity in addition reactions, from the equator to the pole. Indeed, polar 6.6-bonds *ab* have the order equal to 1.60 whereas the *ee* bond order is 0.96 (natural bond orbitals analysis from our previous work [54]; see also the case study represented by the C_{50} fullerene [55]).

We assume that, in addition to fullerenes, such 'distribution of reactivity' (higher reactive atoms to the poles and lower reactive atoms to the equator) is usual for other oblong carbon nanostructures, such as dimers. In the case of fullerenes, the difference in the reactivity could be also explained with the difference in the curvatures of the compared regions of the carbon surface. Usually, polar regions of fullerene molecules are more curved [54,56]. In dimer $(C_{60})_2$ (C_{2h}), low reactivity of the bridging carbon atoms deduced from the topology is due to their sp^3-hybridization. It means that the used topological indices correctly indicate opportunities of addition reactions in the context of the hybridization of the reactive sites. Thus, the topological stability of this kind relates only to the inertness of the reactive sites toward the addition reactions. Indeed, dimer $(C_{60})_2$ (C_{2h}) is able to dissociate forming two separate C_{60} molecules via the C–C bonds [10] classified by topological analysis as stable.

Symmetry is usually invoked when comparing fullerene structures. It is important but insufficient itself to drive fullerene-based compounds toward the most stable structures. The symmetry decreases from C_{120} (D_5) fullerene to classic dimer $(C_{60})_2$ (C_{2h}) and then to peanut C_{120} (C_i). The rotational symmetry numbers (σ) characterizing these symmetry point groups equal $10 > 4 > 1$. Another order is observed for extremal topological roundness and Wiener indices of these structures: C_{120} (D_5) < C_{120} (C_i) < $(C_{60})_2$ (C_{2h}) (Table 1). Comparing these series with the DFT computations, we may postulate that that topological symmetry of these nanostructures matters more the thermodynamic stability as compared with geometrical one.

The σ and ρ^E (or W) trends do not match. Therefore, we conclude that our topological indices relate not to the symmetry but to the shape and fragmentability of molecular systems. The dependence of the Wiener index on the molecular size is well known (see the calculations for 1D lattices (polymers) [57] and their generalization for D-dimensional lattices [58]). Heuristically, it depends on the presence of the node eccentricities in Equation (3).

In this work, we consider three structures comparable in size, so the topological indices ρ^E and W relate to the shape in the following sense. The C_{120} (D_5) with lowest ρ^E and W is an integral structure, viz. it is difficult to select different moieties in it. In contrast, it is easily to select two fullerene cores in the dimer $(C_{60})_2$ (C_{2h}) molecules with the highest ρ^E and W. In this sense, $(C_{60})_2$ (C_{2h}) is fragmentable. Nanopeanut C_{120} (C_i) is intermediate in terms of the ρ^E and W parameters. The hemi-molecules are easier to recognize in the fullerene, but harder than in the classical dimer. Remarkably, the fragmentability trend based on ρ^E and W is consistent with the stability trend based on the DFT computations of the molecular total energies (Table 1).

In the study above, we have operated with global indices W, ρ, and ρ^E, i.e., corresponding to the whole molecules. So far, when calculating the topological indices, we have considered topological interactions within entire graph diameter M. However, it is possible to restrict the range of the topological interactions by applying cut-off parameter k with $1 \leq k \leq M$ that poses the upper limit to the chemical distances $d_{ij} \leq k$, which contribute to the calculations of the invariants Equations (1)–(7).

For example, graph invariant $W(k)$ in the range of k = 6, 7, ... 12, 13 (i.e., limiting the interactions from the 1st till the 6th nearest neighbors in case of k = 6 etc.) privilege the $(C_{60})_2$ (C_{2h}) dimer. Over the interaction range for $k \geq 14$, the other two molecules result in more compact. Particularly, the C_{120} fullerene becomes the most compact at k = 3, 4, 5, and 15 (Figure 2a). Index $\rho(k)$ shows the inversion at k = 6 where $(C_{60})_2$ (C_{2h}) emerges the most round structure whereas C_{120} (D_5) still prevails for the other k values (Figure 2b). The present calculations show that the fullerene cage is also the roundest structure according to the $\rho^E(k)$ index at any value of k.

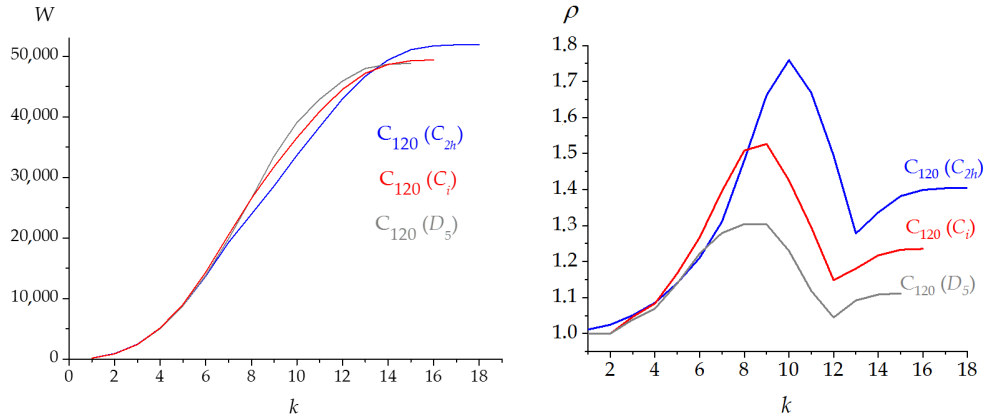

(**a**) (**b**)

Figure 2. Dependences $W(k)$ (**a**) and $\rho(k)$ (**b**) for the isomeric C_{120} structures.

3.2. Linear and Zigzag [2+2]-Linked Oligomers $(C_{60})_n$

We were previously performed a DFT study of the dipole polarizability of the nano-aggregates constructed with the C_{60} cores connected via [2+2]-cycloadditions with all-*trans*-1 (linear oligomers) and all-e_{edge} positions (zigzag oligomers) [23]. In the present work, we study both linear ($n \geq 2$) and zigzag chains $(C_{60})_n$ ($n \geq 3$) in the aspect of their topology (Figures 3 and 4).

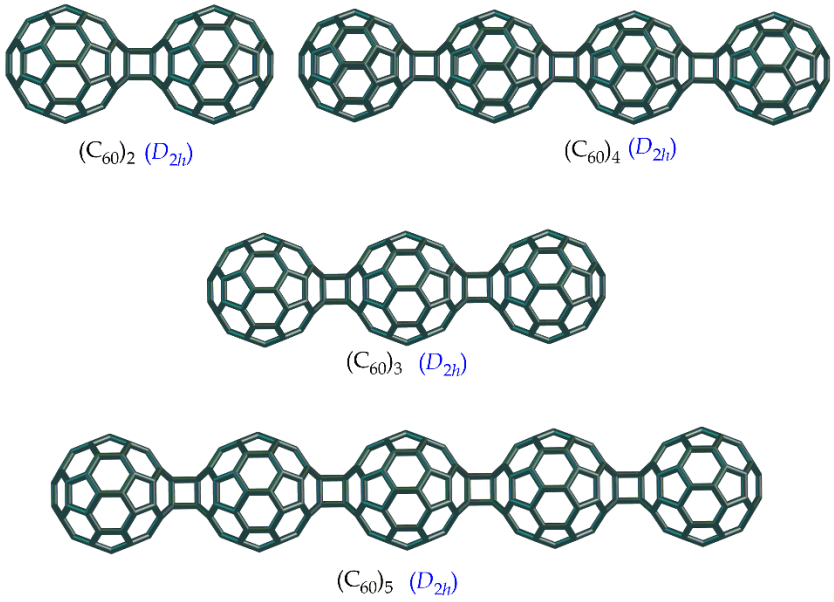

Figure 3. The structures of linear $(C_{60})_n$ oligomers.

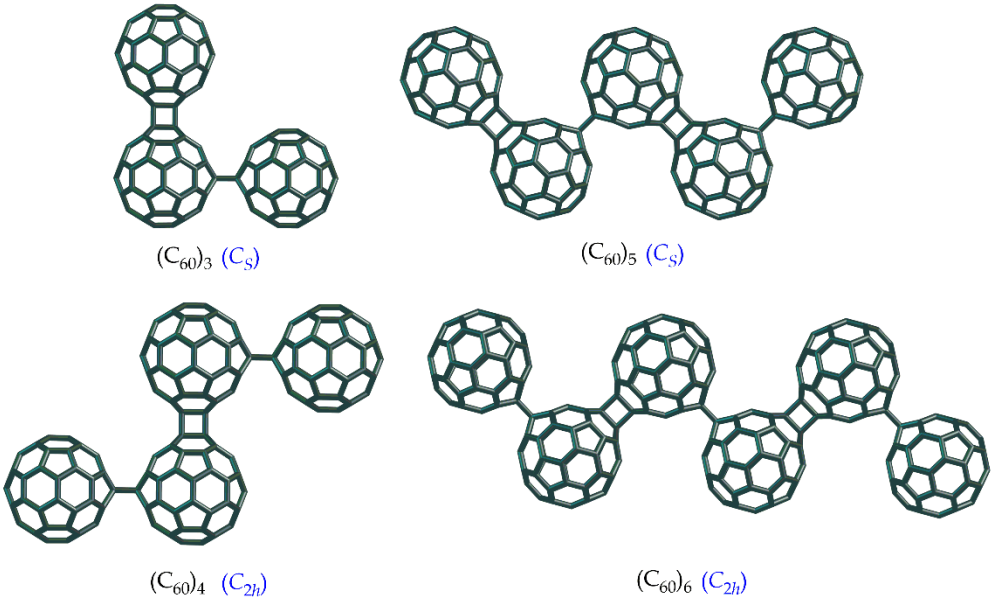

Figure 4. The structures of zigzag $(C_{60})_n$ oligomers.

The results of the calculations are collected in Tables 2 and 3. In general, the *W* values are higher for linear molecules $(C_{60})_n$ as compared with zigzag ones with the same *n*. Hence, index *W* differentiates with oblong (linear) and compact (zigzag) nanostructures (Figures 3 and 4).

Table 2. Topological and information entropy parameters of linear oligomers $(C_{60})_n$.

n	Symmetry Point Group	σ	*W*	ρ	ρ^E	*h* (Bits)
2	D_{2h}	4	51,912	1.4045	1.7792	3.974
3	D_{2h}	4	163,116	1.2639	1.7113	4.603
4	D_{2h}	4	374,352	1.3493	1.8824	4.974
5	D_{2h}	4	718,020	1.3043	1.8501	5.322
6	D_{2h}	4	1,226,520	1.3392	1.9198	5.559

Table 3. Topological and information entropy parameters of zigzag oligomers $(C_{60})_n$.

n	Symmetry Point Group	σ	*W*	ρ	ρ^E	*h* (Bits)
3	C_S	1	149,004	1.4150	1.9231	6.559
4	C_{2h}	2	319,776	1.4451	1.9892	5.974
5	C_S	1	582,948	1.4277	2.0360	7.295
6	C_{2h}	2	960,120	1.4339	2.0323	6.559
7	C_S	1	1,468,572	1.4173	2.0580	7.781

Expectedly, the ρ^E values are higher for compact zigzag oligomers. Interestingly, the view of descriptor function $\rho^E = f(n)$ allows classifying the $(C_{60})_n$ nanostructures depending on their shape, i.e., linear or zigzag (Figure 5). We have found the peculiar odd–even alternation of this function in the case of linear $(C_{60})_n$. Indeed, linear trimer $(C_{60})_3$ manifests the extremal topological roundness lower than that of its even neighbors, i.e., $(C_{60})_2$ and $(C_{60})_4$. In the case of zigzag oligomers, function $\rho^E = f(n)$ has a monotonous behavior with *n*. In general, linear isomers manifest lower topological efficiency being $\rho^E_{linear} < \rho^E_{zigzag}$ (Figure 6a).

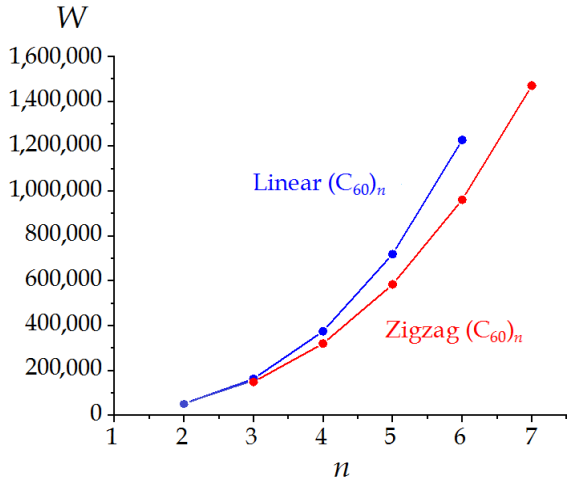

Figure 5. Wiener indices of the $(C_{60})_n$ oligomers.

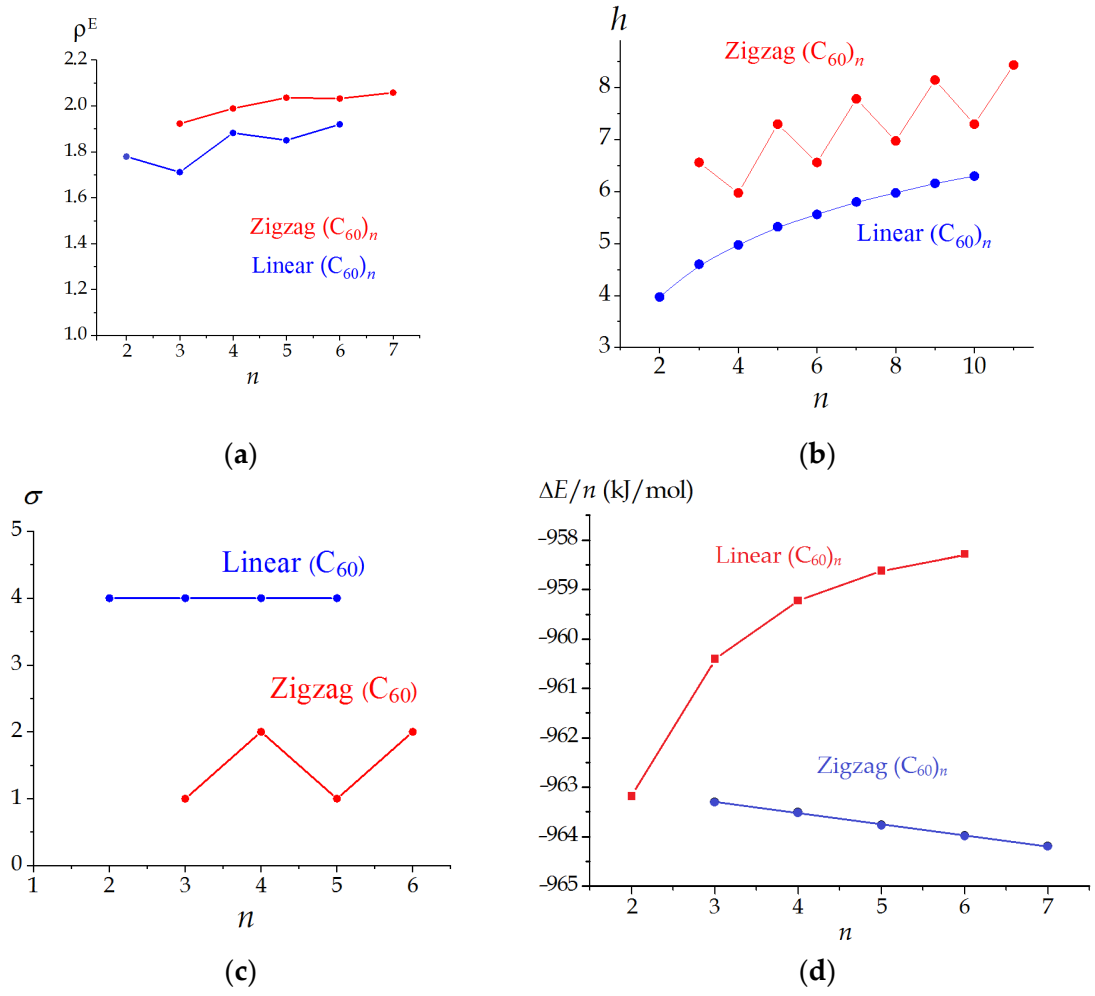

Figure 6. Dependences of extreme topological roundness ρ^E (**a**), information entropy h (**b**), rotational symmetry number σ (**c**) and energy effect of formation (**d**) for linear (blue) and zigzag (red) oligomers $(C_{60})_n$.

As the topological indices of oligomers $(C_{60})_n$ demonstrate odd–even effects, we compared them with other structural descriptors, i.e., information entropy (h) and rotational symmetry number (σ). The first one is an information theoretic index widely used in theoretical chemistry of fullerenes (for example, it was previously used for the analysis of

endofullerene formation [59] and complexity of fullerene graphs [60]). The second one is a characteristic number of symmetry. The information entropy approach treats the molecule as the subsets of inequivalent atoms (their chemical inequivalence corresponds to the positions in the molecular graphs) [61], and the h index is expressed in bits as:

$$h = -\sum_{j=1}^{m} \frac{N_j}{\sum_{j=1}^{m} N_j} \log_2 \frac{N_j}{\sum_{j=1}^{m} N_j}, \quad (9)$$

where m is the number of atom types, N_j are their populations (numbers of atoms attributed to each type), $\Sigma\ N_j = N$ is a total number of atoms in the molecule, $p_j = N_j/\Sigma\ N$ are probabilities to meet the atom of j-th type in the molecular structure.

Based on Equation (9) and analysis of the molecular structure, we have previously derived general relations connecting the information entropy of oligomers $(C_{60})_n$ with n [62]. Their view depends on the addition pattern, linear or zigzag, and oddity–evenness of the n number:

$$h_{linear}^{even} = \frac{1}{15} \log_2 15n + \frac{14}{15} \log_2 \frac{15n}{2}, \quad (10)$$

$$h_{linear}^{odd} = \frac{n+2}{15y} \log_2 15n + \frac{2(7n-1)}{15n} \log_2 \frac{15n}{2}, \quad (11)$$

$$h_{zigzag}^{even} = \frac{14}{15} \log_2 15n + \frac{1}{15} \log_2 30n, \quad (12)$$

$$h_{zigzag}^{odd} = \frac{1}{15} \log_2 60n + \frac{7}{15} \log_2 30n. \quad (13)$$

The calculations via Equations (10)–(13) are shown in Tables 2 and 3. Similar to $\rho^E = f(n)$, the view of dependences $h = f(n)$ depends on the molecular shape of $(C_{60})_n$. However, in contrast to $\rho^E = f(n)$, the information entropy of zigzag oligomers is saw-like, whereas h monotonously increases with n for linear structures (Figure 6b). Herewith, more symmetric even zigzag $(C_{60})_n$ obtain lower h values.

We try rationalizing the non-monotonous behavior of the $\rho^E = f(n)$ and $h = f(n)$ for selected types of the oligomers (linear and zigzag, respectively) through the symmetry of the nanostructures under study. The symmetry point groups of the linear oligomers are constantly D_{2h}, i.e., independent of the number of the fullerene units. In the case of zigzag $(C_{60})_n$, the odd isomers have a C_S symmetry and the even members are C_{2h} structures. These features of the symmetry of $(C_{60})_n$ are illustrated with the function of rotational symmetry number on the size of the nanostructure $\sigma = f(n)$ (Figure 6c). Function $\sigma = f(n)$ is constant for linear isomers $(C_{60})_n$ and oscillates zigzag $(C_{60})_n$. Hence, both ρ^E and h differentiate the series of $(C_{60})_n$ depending on the addition pattern. However, information entropy better reflects the symmetry alternation of the nano-aggregates. We think that this is due to the differences in the protocols of calculating ρ^E and h values. The h index is deduced from the representation of the molecules as a set. In other words, its calculation implies the use of only the vertices of the molecular graph (though the classification of the vertices indirectly uses the connectivity). In contrast, the roundness based on the Wiener indices exploits the edges of the graphs. Based on the obtained results, we consider that representing the $(C_{60})_n$ molecules as the sets is more convenient for rationalizing their symmetries as compared with the representation as networks.

In our studies, we try to reveal correlations between topology, structure, and stability of compounds [34,35]. We have calculated the energy changes upon oligomer formation from n molecules of C_{60}, similar to Equation (8). In the case of the $(C_{60})_n$ nano-aggregates, we do not find correlations between the energy and structural parameters. The energy trends in series of linear and zigzag $(C_{60})_n$ differ: with increasing n, the thermodynamic stability of the linear nanostructures decreases, whereas there is a linear increase for the kinked counterparts (Figure 6d). The unfavourability of the formation of linear polymers of C_{60} has been previously noticed in experimental work [13].

In the previous parts of the present study, we have made molecular symmetry the central point that defines other molecular properties. Here, we note that the molecular symmetry in homologic series $(C_{60})_n$ does not affect the energies because there are no odd–even effects according to the symmetry oscillations. Molecular size and addition pattern (regardless of the symmetry) play crucial roles in the stability trends.

We consider that our numerical estimations of the nano-objects will be further used in digitalizing the structural design approaches of novel materials focused on the chemical structure rather than their thermodynamic stability (see [63–65]).

4. Conclusions and Prospective

We have performed the all-round theoretical study of the fullerene-based covalently bonded nano-aggregates in terms of quantum chemical, structural, topological, and information entropy approaches. The approaches mainly provide consistent estimates and could be further used to predict molecular properties of bulky $(C_{60})_n$ molecules without time- and resource-cost quantum chemical calculations.

As found, the studied topological indices (Wiener index W and topological efficiencies ρ and ρ^E) efficiently describe the molecular shapes (and fragmentability) of isomeric carbon nanostructures C_{120}. Estimated with W and ρ^E, the topological stability (compactness) correlates well with the thermodynamic stability trend obtained with high-level DFT calculations. A detailed analysis of the contributions to molecular descriptor W allows elucidating the most and least reactive atoms of the structure toward the addition reactions. The least reactive atoms make up the equatorial belt in each C_{120} structure. This agrees with experimental data on the reactivity of higher fullerenes and we assume the following general regularity: that the least reactive atoms are located in 'equatorial' parts of oblong fullerenes and related carbon nanostructures.

However, the topological approach does not reflect molecular symmetries of nano-aggregates $(C_{60})_n$ due to its mathematical feature. The symmetry of nano-objects and molecules relates to the spatial positions of atoms whereas the used topological indices are deduced from the topological distances between the vertices of the corresponding molecular graphs. Therefore, we use the information entropy (h) approach to connect the symmetry with structural descriptors. The h values are based on the atom classification, so they 'catch' the symmetry point groups of $(C_{60})_n$ and reproduce odd–even effects on the symmetry.

Note that none of the structural indices correlate with the energy trends of the $(C_{60})_n$ stability (in contrast to the C_{120} case). Thus, in the studied homologic series, linear and zigzag $(C_{60})_n$, molecular size and addition pattern is decisive for energy properties as compared with molecular symmetry.

In further studies, we will search for the correlations between structural descriptors and molecular properties of the fullerene-based nanostructures. This is actual in two aspects. The first one deals with replacing heavy high-level quantum chemical computations of nano-objects, such as $(C_{60})_n$, with faster topological and information theoretic calculations. The second aspect relates to digitalizing carbon nanostructures. For this purpose, we need to create a database covering diverse structural, topological, and other descriptors to make the digital passports of chemical structures.

Author Contributions: Conceptualization, D.S.S., O.O., A.A.T. and I.S.S.; methodology, D.S.S., O.O., A.A.T. and I.S.S.; software, D.S.S., O.O., A.A.T. and I.S.S.; validation, D.S.S., O.O., A.A.T. and I.S.S.; formal analysis, D.S.S., O.O., A.A.T. and I.S.S.; investigation, D.S.S., O.O., A.A.T. and I.S.S.; writing—original draft preparation, D.S.S., O.O., A.A.T. and I.S.S.; writing—review and editing, D.S.S., O.O., A.A.T. and I.S.S.; visualization, D.S.S., O.O., A.A.T. and I.S.S.; project administration, D.S.S. and O.O.; funding acquisition, D.S.S. All authors have read and agreed to the published version of the manuscript.

Funding: D.S.S. is grateful to The President's Grants Council, Russia for financial support (grant number MD-874.2021.1.3).

Institutional Review Board Statement: Not applicable.

Informed Consent Statement: Not applicable.

Acknowledgments: The work was performed under the theme "Novel theoretical approaches and software for modeling complex chemical processes and compounds with tunable physicochemical properties" (registration number AAAA-A19-119022290011-6, Institute of Petrochemistry and Catalysis UFRC RAS).

Conflicts of Interest: The authors declare no conflict of interest.

References

1. Zhechkov, L.; Heine, T.; Seifert, G. D_{5h} C_{50} fullerene: A building block for oligomers and solids? *J. Phys. Chem. A* **2004**, *108*, 11733–11739. [CrossRef]
2. Ariga, K.; Shrestha, L.K. Fullerene nanoarchitectonics with shape-shifting. *Materials* **2020**, *13*, 2280. [CrossRef] [PubMed]
3. Segura, J.L.; Martin, N. [60] Fullerene dimers. *Chem. Soc. Rev.* **2000**, *29*, 13–25. [CrossRef]
4. Komatsu, K.; Wang, G.-W.; Murata, Y.; Tanaka, T.; Fujiwara, K. Mechanochemical synthesis and characterization of the fullerene dimer C_{120}. *J. Org. Chem.* **1998**, *63*, 9358–9366. [CrossRef]
5. Komatsu, K.; Fujiwara, K.; Tanaka, T.; Murata, Y. The fullerene dimer C_{120} and related carbon allotropes. *Carbon* **2000**, *38*, 1529–1534. [CrossRef]
6. Yoshida, M.; Ōsawa, E. Formalized drawing of fullerene Nets. 1. Algorithm and exhaustive generation of isomeric structures. *Bull. Chem. Soc. Jpn.* **1995**, *68*, 2073–2081. [CrossRef]
7. Ueno, H.; Ōsawa, S.; Ōsawa, E.; Takeuchi, K. Stone-Wales rearrangement pathways from the hinge-opened [2+2] C_{60} dimer to Ipr C_{120} fullerenes. Vibrational analysis of intermediates. *Fuller. Sci. Technol.* **1998**, *6*, 319–338. [CrossRef]
8. Takashima, A.; Nishii, T.; Onoe, J. Formation process and electron-beam incident energy dependence of one-dimensional uneven peanut-shaped C_{60} polymer studied using in situ high-resolution infrared spectroscopy and density-functional calculations. *J. Phys. D Appl. Phys.* **2012**, *45*, 485302. [CrossRef]
9. Wang, G.; Li, Y.; Huang, Y. Structures and electronic properties of peanut-shaped dimers and carbon nanotubes. *J. Phys. Chem.* **2005**, *109*, 10957–10961. [CrossRef]
10. Zhu, S.-E.; Li, F.; Wang, G.-W. Mechanochemistry of fullerenes and related materials. *Chem. Soc. Rev.* **2013**, *42*, 7535–7570. [CrossRef]
11. Kunitake, M.; Uemura, S.; Ito, O.; Fujiwara, K.; Murata, Y.; Komatsu, K. Structural analysis of C_{60} trimers by direct observation with scanning tunneling microscopy. *Angew. Chem.* **2002**, *114*, 1011–1014. [CrossRef]
12. Ohtsuki, T.; Masumoto, K.; Tanaka, T.; Komatsu, K. Formation of dimer, trimer, and tetramer of C_{60} and C_{70} by γ-ray, charged-particle irradiation, and their HPLC separation. *Chem. Phys. Lett.* **1999**, *300*, 661–666. [CrossRef]
13. Sun, D.; Reed, C.A. Crystal engineering a linear polymer of C_{60} fullerene *via* supramolecular pre-organization. *Chem. Commun.* **2000**, 2391–2392. [CrossRef]
14. Chadli, H.; Rahmani, A.; Sbai, K.; Hermet, P.; Rols, S.; Sauvajol, J.-L. Calculation of Raman-active modes in linear and zigzag phases of fullerene peapods. *Phys. Rev. B* **2006**, *74*, 205412. [CrossRef]
15. Lee, J.Y.; Lee, C.; Ōsawa, E.; Choi, J.W.; Sur, J.C.; Lee, K.H. Snapshots of the fragmentation for C_{70}@single-walled carbon nanotube: Tight-binding molecular dynamics simulations. *Int. J. Mol. Sci.* **2021**, *22*, 3929. [CrossRef]
16. Lee, C.; Lee, J.Y.; Ōsawa, E.; Lee, K.H. A conversion dynamics of $(C_{60})_2$ dimer fullerenes to a fused dimer cage in carbon nanopeapods: Tight-binding molecular dynamics simulation. *Bull. Korean Chem. Soc.* **2019**, *40*, 1054–1055. [CrossRef]
17. Glukhova, O.E.; Kolesnikova, A.S.; Kirillova, I.V. Investigation of the effect of bending on the polymerization of fullerenes inside carbon nanotubes. *Fuller. Nanotub. Carbon Nanostruct.* **2012**, *20*, 391–394. [CrossRef]
18. Ōsawa, S.; Sakai, M.; Ōsawa, E. Nature of cyclobutane bonds in the neutral [2+2] dimer of C_{60}. *J. Phys. Chem. A* **1997**, *101*, 1378–1383. [CrossRef]
19. Ōsawa, S.; Ōsawa, E.; Hirose, Y. Doubly bonded C_{60} dimers and congeners: Computational studies of structures, bond energies and transformations. *Fuller. Sci. Technol.* **1995**, *3*, 565–585. [CrossRef]
20. Bihlmeier, A.; Samson, C.C.M.; Klopper, W. DFT study of fullerene dimers. *ChemPhysChem* **2005**, *6*, 2625–2632. [CrossRef]
21. Sabirov, D.S. Polarizability of C_{60} fullerene dimer and oligomers: The unexpected enhancement and its use for rational design of fullerene-based nanostructures with adjustable properties. *RSC Adv.* **2013**, *3*, 19430–19439. [CrossRef]
22. Sabirov, D.S.; Terentyev, A.O.; Bulgakov, R.G. Polarizability of fullerene [2 + 2]-dimers: A DFT study. *Phys. Chem. Chem. Phys.* **2014**, *16*, 14594–14600. [CrossRef] [PubMed]
23. Pankratyev, E.Y.; Tukhbatullina, A.A.; Sabirov, D.S. Dipole polarizability, structure, and stability of [2+2]-linked fullerene nanostructures $(C_{60})_n$ ($n \leq 7$). *Phys. E* **2017**, *86*, 237–242. [CrossRef]
24. Ma, F.; Li, Z.-R.; Zhou, Z.-J.; Wu, D.; Li, Y.; Wang, Y.-F.; Li, Z.-S. Modulated nonlinear optical responses and charge transfer transition in endohedral fullerene dimers Na@$C_{60}$$C_{60}$@F with *n*-fold covalent bond (n = 1, 2, 5, and 6) and long range ion bond. *J. Phys. Chem. C* **2010**, *114*, 11242–11247. [CrossRef]

25. Tukhbatullina, A.A.; Shepelevich, I.S.; Sabirov, D.S. Exaltation of polarizability as a common property of fullerene dimers with diverse intercage bridges. *Fuller. Nanotub. Carbon Nanostruct.* **2018**, *26*, 661–666. [CrossRef]
26. Kaur, S.; Sharma, A.; Sharma, H.; Dhiman, S.; Mudahar, I. Substitutional doping of symmetrical small fullerene dimers. *Int. J. Quantum Chem.* **2019**, *119*, e26019. [CrossRef]
27. Swart, M.; van Duijnen, P.T. Rapid determination of polarizability exaltation in fullerene-based nanostructures. *J. Mater. Chem. C* **2015**, *3*, 23–25. [CrossRef]
28. Silva, R.A.L.; de Brito, S.F.; Machado, D.F.S.; Carvalho-Silva, V.H.; de Oliveira, H.C.B.; Ribeiro, L. The influence of the configuration of the $(C_{70})_2$ dimer on its rovibrational spectroscopic properties: A theoretical survey. *J. Mol. Model.* **2018**, *24*, 235. [CrossRef]
29. Schwerdtfeger, P.; Wirz, L.N.; Avery, J. The topology of fullerenes. *WIRES Comput. Mol. Sci.* **2015**, *5*, 96–145. [CrossRef]
30. Sure, R.; Hansen, A.; Schwerdtfeger, P.; Grimme, S. Comprehensive theoretical study of all 1812 C_{60} isomers. *Phys. Chem. Chem. Phys.* **2017**, *19*, 14296–14305. [CrossRef]
31. Ori, O.; Cataldo, F.; Graovac, A. Topological ranking of C_{28} fullerenes reactivity. *Fuller. Nanotub. Carbon Nanostruct.* **2009**, *17*, 308–323. [CrossRef]
32. Vukicevic, D.; Cataldo, F.; Ori, O.; Graovac, A. Topological efficiency of C_{66} fullerene. *Chem. Phys. Lett.* **2011**, *501*, 442–445. [CrossRef]
33. Ori, O.; D'Mello, M. A topological study of the structure of the C_{76} fullerene. *Chem. Phys. Lett.* **1992**, *197*, 49–54. [CrossRef]
34. Sabirov, D.S.; Ori, O.; Laszlo, I. Isomers of the C_{84} fullerene: A theoretical consideration within energetic, structural, and topological approaches. *Fuller. Nanotub. Carbon Nanostruct.* **2018**, *26*, 100–110. [CrossRef]
35. Dobrynin, A.A.; Ori, O.; Putz, M.V.; Vesnin, A.Y. Generalized topological efficiency—Case study with C_{84} fullerene. *Fuller. Nanotub. Carbon Nanostruct.* **2020**, *28*, 545–550. [CrossRef]
36. Bultheel, A.; Ori, O. Topological modeling of 1-Pentagon carbon nanocones—Topological efficiency and magic sizes. *Fuller. Nanotub. Carbon Nanostruct.* **2018**, *26*, 291–302. [CrossRef]
37. Sabirov, D.S.; Ori, O. Skeletal rearrangements of the C_{240} fullerene: Efficient topological descriptors for monitoring Stone–Wales transformations. *Mathematics* **2020**, *8*, 968. [CrossRef]
38. Laikov, D.N.; Ustynyuk, Y.A. PRIRODA-04: A quantum-chemical program suite. New possibilities in the study of molecular systems with the application of parallel computing. *Russ. Chem. Bull.* **2005**, *54*, 820–826. [CrossRef]
39. Chemcraft. Available online: http://www.chemcraftprog.com (accessed on 7 October 2021).
40. Stück, D.; Baker, T.A.; Zimmerman, P.; Kurlancheek, W.; Head-Gordon, M. On the nature of electron correlation in C_{60}. *J. Chem. Phys.* **2011**, *135*, 194306. [CrossRef]
41. Chai, J.-D. Density functional theory with fractional orbital occupations. *J. Chem. Phys.* **2012**, *136*, 154101. [CrossRef]
42. Chai, J.-D. Thermally-assisted-occupation density functional theory with generalized-gradient approximations. *J. Chem. Phys.* **2014**, *140*, 18A521. [CrossRef]
43. Chai, J.-D. Role of exact exchange in thermally-assisted-occupation density functional theory: A proposal of new hybrid schemes. *J. Chem. Phys.* **2017**, *146*, 044102. [CrossRef] [PubMed]
44. Sheka, E.F.; Zaets, V.A. The radical nature of fullerene and its chemical activity. *Russ. J. Phys. Chem. A* **2005**, *79*, 2009–2015.
45. Tuktarov, A.R.; Akhmetov, A.R.; Sabirov, D.S.; Khalilov, L.M.; Ibragimov, A.G.; Dzhemilev, U.M. Catalytic [2+1] cycloaddtion of diazo compounds to [60] fullerene. *Russ. Chem. Bull.* **2009**, *58*, 1724–1730. [CrossRef]
46. Sabirov, D.S.; Terentyev, A.O.; Bulgakov, R.G. Counting the isomers and estimation of anisotropy of polarizability of the selected C_{60} and C_{70} bisadducts promising for organic solar cells. *J. Phys. Chem. A* **2015**, *119*, 10697–10705. [CrossRef] [PubMed]
47. Kuznetsov, V.V. Stereochemistry of simple molecules inside nanotubes and fullerenes: Unusual behavior of usual systems. *Molecules* **2020**, *25*, 2437. [CrossRef]
48. Diniakhmetova, D.R.; Friesen, A.K.; Kolesov, S.V. Quantum chemical modeling of the addition reactions of 1-*n*-phenylpropyl radicals to C_{60} fullerene. *Int. J. Quantum Chem.* **2016**, *116*, 489–496. [CrossRef]
49. Shestakov, A.F. Role of fullerene–nitrogen complexes of alkali metals in C_{60}-catalyzed nitrogen fixation. *Russ. J. Phys. Chem. A* **2020**, *94*, 919–924. [CrossRef]
50. Pankratyev, E.Y.; Tulyabaev, A.R.; Khalilov, L.M. How reliable are GIAO calculations of ^{1}H and ^{13}C NMR chemical shifts? A statistical analysis and empirical corrections at DFT (PBE/3z) level? *J. Comput. Chem.* **2011**, *32*, 1993–1997. [CrossRef]
51. Iranmanesh, A.; Ashrafi, A.R.; Graovac, A.; Cataldo, F.; Ori, O. Wiener index role in topological modeling of hexagonal systems–from fullerenes to graphene. In *Distance in Molecular Graphs—Applications*; Gutman, I., Furtula, B., Eds.; University Kragujevac: Kragujevac, Serbia, 2012; pp. 135–155.
52. Ōsawa, E. Formation mechanism of C_{60} under nonequilibrium and irreversible conditions—An annotation. *Fuller. Nanotub. Carbon Nanostruct.* **2012**, *20*, 299–309. [CrossRef]
53. Sabirov, D.S.; Bulgakov, R.G.; Khursan, S.L. Indices of the fullerene reactivity. *ARKIVOC* **2011**, *2011*, 200–224. [CrossRef]
54. Sabirov, D.S.; Khursan, S.L.; Bulgakov, R.G. 1,3-Dipolar addition reactions to fullerenes: The role of the local curvature of carbon surface. *Russ. Chem. Bull.* **2008**, *57*, 2520–2525. [CrossRef]
55. Graovac, A.; Ashrafi, A.R.; Ori, O. Topological efficiency approach to fullerene stability—Case study with C_{50}. *Adv. Math. Chem. Appl.* **2015**, *2*, 3–23. [CrossRef]
56. Lu, X.; Chen, Z. Curved pi-conjugation, aromaticity, and the related chemistry of small fullerenes ($<C_{60}$) and single-walled carbon nanotubes. *Chem. Rev.* **2005**, *105*, 3643–3696. [CrossRef] [PubMed]

57. Bonchev, D.; Mekenyan, O. A topological approach to the calculation of the π-electron energy and energy gap of infinite conjugated polymers. *Z. Nat. A* **1980**, *35*, 739–747. [CrossRef]
58. Cataldo, F.; Ori, O.; Iglesias-Groth, S. Topological lattice descriptors of graphene sheets with fullerene-like nanostructures. *Mol. Simul.* **2010**, *36*, 341–353. [CrossRef]
59. Sabirov, D.S.; Terentyev, A.O.; Sokolov, V.I. Activation energies and information entropies of helium penetration through fullerene walls. Insights into the formation of endofullerenes nX@$C_{60/70}$ (n = 1 and 2) from the information entropy approach. *RSC Adv.* **2016**, *6*, 72230–72237. [CrossRef]
60. Ghobani, M.; Dehmer, M.; Emmert-Streib, F. Properties of entropy-based topological measures of fullerenes. *Mathematics* **2020**, *8*, 740. [CrossRef]
61. Sabirov, D.S. Information entropy changes in chemical reactions. *Comput. Theor. Chem.* **2018**, *1123*, 167–179. [CrossRef]
62. Sabirov, D.S. Information entropy change in [2+2]-oligomerization of the C_{60} fullerene. *Int. J. Chem. Model.* **2017**, *9*, 203–213.
63. Feng, B.; Zhuang, X. Carbon-enriched meso-entropy materials: From theory to cases. *Acta Chim. Sin.* **2020**, *78*, 833–847. [CrossRef]
64. Diana, N.; Yamada, Y.; Gohda, S.; Ono, H.; Kubo, S.; Sato, S. Carbon materials with high pentagon density. *J. Mater. Sci.* **2021**, *56*, 2912–2943. [CrossRef]
65. Champion, Y.; Thurieau, N. The sample size effect in metallic glass deformation. *Sci. Rep.* **2020**, *10*, 10801. [CrossRef] [PubMed]